Damage characterization in composite materials using acoustic emission signal-based and parameter-based data

Damage Characterization in Composite Materials using Acoustic Emission Signal-based and Parameter-based data

Claudia Barile[a]*, Caterina Casavola[a], Giovanni Pappalettera[a], Paramsamy Kannan Vimalathithan[a]

[a]*Dipartimento Meccanica, Matematica e Management, Politecnico di Bari, Viale Japigia 182, 70126 Bari, Italy*

Paper submitted for publication in

COMPOSITES PART B: ENGINEERING

**Author to whom the correspondence to be addressed*

Dr. Claudia Barile,

Dipartimento di Meccanica Matematica e Management,

Politecnico di Bari, Viale Japigia 182, 70126 Bari, Italy.

Email ID: claudia.barile@poliba.it

Damage Characterization in Composite Materials using Acoustic Emission Signal-based and Parameter-based data

Claudia Barile[a]*, Caterina Casavola[a], Giovanni Pappalettera[a], Paramsamy Kannan Vimalathithan[a]

[a]*Dipartimento Meccanica, Matematica e Management, Politecnico di Bari, Viale Japigia 182, 70126 Bari, Italy*

Abstract

Damage propagation in DCB specimens is characterized by Acoustic Emission (AE) Technique. Signal-based AE data is used to relate the Mechanical Property of the Material with the Acoustic Activity; Sentry function is used to relate the Strain Energy and Acoustic Energy. The cumulative acoustic energy provides information about the critical points before failure in each specimen. Nonetheless, it was observed that the Sentry function reveals concealed information about the damage propagation and material deterioration which are concealed in the Load-Displacement curve. Sentry function can be used to characterize the damage propagation in material even before its critical point of failure. The signal-based data, the wavelets, are decomposed into different levels using the Wavelet Packet Transform (WPT). These WPT results discriminate the different frequency band associated with the different types of damage propagation. The false signals from both the mechanical results and acoustic results can be identified using the WPT results.

Keywords: A. Polymer-matrix composites (PMCs); A. Carbon fibers; D. Acoustic emission; C. Damage mechanics

1. Introduction

Acoustic Emission (AE) has become one of the most sought Non-Destructive Evaluation (NDE) techniques in structural health monitoring over the past few decades. The AE technique is regarded as the most efficient 'Passive' NDE tool. The term 'Passive' refers to the fact that an artificial signal source is not required for the AE technique. It rather receives the source signals from the material being tested in the form of spontaneous release of energy (burst signals). There has been some rhetorical dispute whether AE technique is Non-Destructive or not. These trivial disagreements can be rather ignored as AE provides In-Situ information during the testing. Unlike the other NDE tools, where the material can be characterized before and (or) after the testing, AE provides the feasibility

to continuously monitor the material under loading. Thus, AE can be used to detect or predict the failure of a specimen or a structure at a very early stage [1].

The most unique aspect of the AE technique is that the damage progress in a material throughout its entire load history can be monitored and tested [1,2]. This provides the continuous monitoring of a material or structure under loading, with the enormous amount of data to be stored during the entire process is the only trifling disadvantage [3]. The advances in the computing and the modern-day storage devices have made AE to overcome this limitation, thus, providing the online monitoring of the material or structure under continuous loading. Moreover, the AE provides the information on the material during testing in two different modes: Parameter-based results and Signal-based results. The AE parameters such as Peak Amplitude, Peak Energy, Counts, Hits, Time of Arrival and Rise Time (can be collectively known as AE descriptors) have been successfully used by many researchers over the years to characterize the damage processes in composite materials, metals and their respective structures [4-8]. Some researchers have, however, argued that the Peak Amplitude is an unreliable parameter in the damage monitoring using AE [9,10]. Although Peak Amplitude is the absolute measured which is not influenced by the system gain or threshold gain, only by the pre-amplifier gain, the attenuation and wide variation in rise time with respect to the propagation distance, makes it an unreliable parameter in most instances [9-11].

However, the parameter-based AE monitoring provides a significant amount of information on the damage progression. Several researchers have formulated numerical models to characterize the damage progression in composite materials and metals only with the AE descriptors [12-15]. Some researchers have formulated numerical models by relating the Acoustic Energy and Strain Energy released by the Fiber Reinforced Plastics (FRP) under loading to characterize the damage mechanism, while some other authors have formulated models to estimate the crack growth in metals [17,18]. There are reports on estimating the fatigue life of the FRP materials using numerical analysis of AE descriptors. However, the AE descriptors have been extensively used in structural monitoring and damage progression in concrete and rock structures rather than FRPs and Metals [19-21]. Particularly, the Natural Time (NT) analysis has been used on the quasi-brittle materials. This method has used the acoustic counts per hit as a function to unveil the hidden information in time series. However, the mechanical results and the acoustic results has not been related in their

study [22-24]. The Acoustic Parameters must be related to the Mechanical Characteristics of the Material. The most famous numerical model to relate the Acoustic Energy and the Strain Energy released by the Material under loading is the Sentry Function [17]. Sentry Function provides a simple way to relate the acoustic activities with the mechanical characteristics of the material. More details about the Sentry Function has been provided in the subsequent sections. This method has been used frequently in characterizing Glass Fiber Reinforced Plastics (GFRP) under the tensile or compressive loading. Nonetheless, it has rarely been used for Mode I delamination tests. The probable reason is that the material loses its load carrying capacity almost immediately as the ply is delaminated from the FRP structure. Thus, the Sentry Function could not provide much information after the initial delamination. However, it will be interesting to study the Sentry Function for the Mode I delamination tests.

AE descriptors (Parameter-based results) has some limitations, particularly in Mode I delamination tests, albeit being economical and high data storing speeds. Moreover, it is quite difficult to discriminate the AE event signals and the noise signals with the AE descriptors.

AE events normally must be pre-amplified and are influenced by the system gain and threshold gain. It is not quite possible to discriminate the different wave modes related to compression, shear or surface waves. Moreover, the signal to noise ratio discrimination of waveforms is not possible using parameter-based data. However, while using the Signal-based AE analysis, various algorithms and data filtering techniques can be used to enhance the Signal-based data [25-27]. Moreover, it is easy to discriminate the noise signals using the Waveform Analysis. The Waveforms carry more useful information when compared to the AE descriptors and proper analysis of the Waveform can provide more details on the online monitoring of the damage progression in materials. The recorded Waveform of the Acoustic Event that carries the information of the energy burst during the event is generally affected by the medium that propagates the elastic energy, propagation path and the medium, physical nature of the material and the system used for acquisition. However, by using Wavelet Analysis, the appropriate signal can be discriminated and filtered for further analysis. Generally, the acoustic signals are affected by the propagating distance from the source to the sensor due to their highly dispersive nature. Due to their dispersive nature, the properties of the signal in time domain are greatly affected [28]. This forces the researchers to study the AE signal waveforms

in frequency domain. Most of the researchers have used the Fast Fourier Transform (FFT) or the Wavelet to analyse the Waveform in frequency domain [26,27]. It provides instantaneous results by providing the peak frequency. This serves as a powerful online tool to get in-situ information of the AE events during the entire load history. However, this has a major disadvantage. The peak frequency cannot represent the true nature of the AE signal. Peak frequency represents the single highest frequency point of the entire spectrum. This is a reliable parameter considering the spectrum contains only one frequency content. The AE signals always have several frequency content and considering the peak frequency is not appropriate [29]. For this reason, the wavelets of AE signals are to be analysed in frequency-time domain. The Wavelet Analysis provides more information on the Frequency-Time domain. Conventionally, the two types of commonly used Wavelet Analysis are Continuous Wavelet Transform (CWT) and Discrete Wavelet Transform (DWT). CWT provides more details on the Frequency-Time domain, whereas, DWT can filter the Wavelet to its lowest Frequency levels to filter out the noise signals. While both CWT and DWT have their advantages over one another, they have quite a few limitations [27]. The advantages and limitations of CWT and DWT can be found elsewhere [30,31].

Only in recent times, the Wavelet Packet Transform (WPT) has become quite popular for Signal-based AE analysis. The WPT decomposes the Waveform into different frequency levels and analysis each component of it in the Frequency-Time domain. It essentially overcomes the limitation of both CWT and DWT in the sense and providing more information. During the online monitoring of a damage progression or a material under testing, the WPT will play a crucial role in decomposing the noise signal effectively and also providing information on the Time-Frequency domain.

Only a few researchers have used WPT in monitoring damage progression in FRPs. Some of the notable works are on classifying the damage mechanism in the evolution of Barely Visible Impact Damage (BVID) in Carbon Fiber Reinforced Plastics (CFRP) and Mode I delamination in E-Glass FRPs [32,33]. Only a one substantial work has been reported on analysing the damage mechanism of Mode I delamination in CFRP [34] using WPT, let alone using the advanced MATLAB® Wavelet Tool Box.

This research work focuses on monitoring and characterizing the CFRP specimens tested under Mode I delamination condition. The Mechanical behaviour and the Acoustic activity are related by the Sentry function. The advanced Wavelet Tool Box in MATLAB® has been used for decomposing

the wavelet and providing a histogram of the decomposed Wavelets in Time-Frequency domain. Moreover, the energy content of the Wavelets has been analysed, after decomposing, to characterize the type of damage mechanism during the Mode I Test.

2. Materials and Methods

2.1 Sentry Function

Sentry function relates the Acoustic and Mechanical Information of the material under loading. It is the logarithm of the ratio between the Cumulative Acoustic Energy released to the Energy stored by the material under loading. The Sentry function is given by the equation [14],

$$f(x) = \ln \frac{E_s(x)}{E_a(x)} \quad (1)$$

where, x usually represents the test-driving variable, displacement or strain. In the present research work, Mode I delamination test is conducted under displacement-controlled mode. Thus, the x represents the displacement in this context. The Sentry Function is generally discontinuous and it has four different patterns which represent different material behaviour. More details about the four distinct patterns and its relation to the Mechanical behaviour of the Material can be found elsewhere [17, 34-37]. Including all the details under the section will water down the core details of the presented research work.

2.2 Wavelet Packet Transform

Wavelet packets are linear combinations or superpositions of wavelets which retains the orthogonality, smoothness and localization properties of their parent [27]. WPT involves decomposing the parent Wavelet into low-frequency component (called Approximation) and a high-frequency component (called Detail). Each of these components is again decomposed into Approximation and Detail until the desired level of decomposition is achieved. The Wavelet Packet Tree of decomposition is provided in Figure 1.

Figure 1. *Wavelet Packet Tree representing L – Low Frequency (Approximation) and H – High Frequency (Detail)*

The number of components (n) for each level is given by 2^i, where i is the decomposition level. The energy of each component in the specific decomposition level can be calculated by Equation (2) [37].

$$E_i^n = \sum_{T=t_0^n}^{t_1^n} \left[f_i^n(T) \right] \quad (2)$$

where, $E_i^n$is the Energy of each component, f_i^n is the WPT component and t_0^n and t_1^n is the time period. The Energy Percentage ($\%_i^n$) of each individual component of the original signal can be calculated using Equation (3) [37].

$$\%_i^n = {E_i^n} \Big/ {\sum_i \sum_n^{2^{i-1}} E_i^n} \quad (3)$$

Each WPT component f_i^n can be derived from the WPT analysis in MATLAB using Wavelet Toolbox. MATLAB provides the feasibility to choose the decomposition level *i*. In this present research work, the Wavelets were decomposed to the level $i = 3$. The sampling rate was set as $f_s = 1\ MSPS$.

2.3 Testing Methods

In this study, the WPT is used for characterizing the damage progression in Double Cantilever Beam (DCB) Specimens. The DCB specimens were made as per ASTM D5528 standard: the length and breadth of each specimen are 125 mm and 25 mm, respectively and the thickness is 3 mm. The specimens were fabricated with an even number of unidirectional plies with a ply thickness of 0.152 mm. A non-adhesive insert of 45 mm long and thickness 13 µm (approx.) is inserted during the curing process, located at the middle of the sample through its thickness to initiate the Mode I delamination. A couple of Piano Hinges were adhered to the surface of the specimen, near the edge of the surface where the insert was positioned, through a strong adhesive. The delamination propagation was along the 0° direction. The schematic of the DCB Specimen tested is given in Figure 2. The DCB test was carried out at room temperature (~ 23 °C) on an INSTRON (Servo-Hydraulic) testing machine. The test was carried out in displacement-controlled mode at a constant displacement rate of 1 mm/min. Three DCB specimens (named A, B and C) were taken for this study.

Figure 2. *Schematic of DCB Specimen with Piano Hinges*

The delaminating crack length was monitored using a CCD camera by recording images at 12.75 frames/s and by overlapping the images recorded with a calibrated grid (Figure 3). The calibration grid was separated into two sections, the blue section representing the initial delamination length

(which corresponds to the length of the insert) and the red section represents the actual delamination length.

Figure 3. *Sample Image recorded through CCD camera with Calibrated Grid*

To record the Acoustic Events during the test, a piezoelectric sensor was coupled to the surface of the specimen through silica gel. Since the surface roughness of the specimen affects the sensor performance in recording the resonances and reverberations, it is necessary to couple the sensor through a suitable couplant (in this case, silica gel). The sensor used in this study is R30α, supplied by Mistras, Physical Acoustics Corporation (PAC). It is a high sensitivity hybrid sensor with a peak sensitivity of 54 dB and an operating frequency ranging between 200 and 750 kHz. The sensor was connected to the PCI-2 data acquisition board not before pre-amplifying the signal by 40 dB through 20/40/60 AST Preamplifier.

Both the parameter-based data and signal-based data are recorded during the tests. The Parameter-based data are essential for identifying the Acoustic Hits and Counts, nonetheless, more emphasis on this present investigation is given to the signal-based data (waveforms).

3. Results and Discussions

3.1 DCB Test Results

From the Load-Displacement curve in Figure 4, it is possible to observe that the damage did not progress in the same way for all 3 specimens, despite their similar geometrical and material similarities. Specimen A exhibits a peak load of 96.26 N, while Specimen B and Specimen C have 97.80 N and 115.70 N, respectively.

Figure 4. *Load-Displacement for Specimens A, B and C*

The non-adhesive insert inside the specimen, its dimension and the ply where it is placed between possibly could affect the Mode I delamination. Another factor that can be attributed to the variation in the Load-Displacement curve is the attachment of piano hinges to the upper and lower plies. The adhesive force with which the hinges are attached to the specimen surface and the curing conditions of the adhesive also plays a significant role in the Mode I Delamination properties of the specimen. Moreover, the fiber pull-out from the adjacent ply during the delamination, the initiation and the propagation of the crack also play a major role in determining the delamination strength. Thus, the

variation in the Peak Load and different peaks observed in the Load-Displacement curve can be justified.

The Load vs Time plot of each DCB test results was combined with the Cumulative number of Hits acquired the Acoustic Events. Since the test is conducted in the displacement-controlled mode, the energy measured from the area under the Load-Displacement curve can be related to the Acoustic Energy. The over-plotted results of the test specimens A, B and C are presented in Figure (5), (6) and (7), respectively.

3.2 Acoustic Emission Results

The Load-Displacement curve for Specimens A, B and C, respectively, are overplotted with the Cumulative Acoustic Energy recorded during the Acoustic Events. Each of them was segmented to three regions based on the different peaks in the Load-Displacement curve. However, in Specimen C, there is only one peak can be observed, nonetheless, is segmented into three regions for the purpose of comparison.

When looking at the Cumulative Acoustic Energy and the Load-Displacement curve, it can be observed that the critical point before failure can easily be identified using Acoustic Energy. For instance, in Specimen A, the Cumulative Acoustic Energy increases rapidly around 90 s duration and increases until 125 s. Further beyond that point, it increases linearly. When comparing it with the Load-Displacement curve, the peak load can be observed at 100 s duration and beyond that, the material starts to lose its load carrying capability.

Figure 5. *Load vs Time and Cumulative Hits vs Time for Specimen A*

Similarly, for Specimen B, the Acoustic Energy increases rapidly from 90 s and the peak load can also be observed at the same time duration. In the case of Specimen C, the Acoustic Energy increases rapidly from 100 s, while the peak load can be observed around 90 s. In each case, the critical point of the load before the material failure can be identified by the acoustic activity. This means that the Cumulative Acoustic Energy is the reliable parameter to understand the critical point of failure during Mode I delamination.

Figure 6. *Load vs Time and Cumulative Hits vs Time for Specimen B*

Figure 7. *Load vs Time and Cumulative Hits vs Time for Specimen C*

3.3 Sentry Function Results

Understanding the critical point of failure is essential albeit not recommendable in practical applications, such as in an Aircraft Structure. It is necessary to understand the initiation and propagation of damage in a structure before failure. Acoustic Emission parameters are very reliable in such applications, especially when it can be related to the Mechanical Properties of the Material. Sentry Function provides the possibility to relate the Cumulative Acoustic Energy and the Strain Energy of the Material under loading. In Figures 8, 9 and 10, the Sentry Function over the crosshead displacement has been compared with the Crack Length.

Figure 8. *Sentry Function and Crack Length Progression for Specimen A*

For Specimen A, three Load Peaks, each in one Region can be observed in Figure 5, with the Peak with the Maximum Load is on Region 3 around 100 s duration. The crack length at the duration of 90 s is close to 25 mm. The crack length 25 mm represents the 2 mm opening of the delaminating crack beyond the length of the insert (the true length of the insert is 45 mm but only 23 mm is included in the calibrated grid for observation; Refer Figure 3). Despite the maximum peak load is at Region 3 around 90 s duration, a steep drop in Sentry function can be observed around 20 s duration. Beyond that point, the Sentry Function gradually increases implying that the material is trying to retain its property. When looking at the images captured using the CCD camera during the crack propagation, the movement in the piano hinges was observed at the early stages of testing (Refer Supplementary Material). The piano hinges were not totally unhinged but probably the adhesive holding the hinges to the surface of the specimen had experienced some cracking or damage, which resulted in both the acoustic activity and mechanical activity. This probably is the reason for the load drop in Region 1 and Region 2 (Figure 5). The acoustic signal does not represent the mechanical failure of material at 20 s duration which is why the Sentry function gradually increased beyond the point. This is one of the implications that Sentry function is one of the powerful tools in characterizing the damage propagation in materials.

Nonetheless in Specimen B, a steep drop in the Sentry Function around 90 s duration (crack length of 24 mm) and its gradual decrease beyond that point (Figure 9). When it reaches the duration of 90 s, the Sentry Function starts decreasing gradually, again indicating the deterioration of the Specimen to failure. It should be noted that both Specimen A and B have a lower peak load when compared to Specimen C. Specimen B started losing it property at an earlier stage when compared to both

Specimen A and C. The duration at which the Peak load can be observed and also the point at which the sentry function gradually started to decrease indicates the same.

Figure 9. *Sentry Function and Crack Length Progression for Specimen B*

In both cases of Specimens A and B, it is evident that by relating the Acoustic Parameter and Strain Energy, more useful and concealed information about the Material can be obtained. Specimen C, by far the best specimen among the three, has a unique case while observing the Load-Displacement curve in Figure 10. It has only one Load Peak around 100 s duration and beyond that point, the load decreases. However, the Sentry Function in Figure 10 shows that after the steep drop at 100 s duration, there persist some sudden outbursts of Acoustic Energy, which can be identified by the subsequent drops in Sentry Function (at 105 s and 150 s). These can be attributed to the opening of the crack length and the propagation of crack length through the Specimen. The Crack Length at the point of drop in the Sentry Function is 24 mm.

Figure 10. *Sentry Function and Crack Length Progression for Specimen C*

From these observations, it is quite evident that the Sentry Function is a reliable tool to relate the Acoustic Activity with the Material Property under loading. One of the major questions that can arise from the Sentry Function is the lack of activity in the Sentry function beyond the point of 100 s duration in all the 3 Specimens. Upon studying the literature based on Sentry Function, normally, the Sentry Function is discontinuous with different patterns as mentioned in the Materials and Methods Section. However, in case of the DCB Specimens A, B and C, there is no significant change in the Sentry Function beyond 100 s duration. The probable reason is that the Mode I delamination requires very less energy to occur and the material starts losing its load carrying capability completely beyond that point, which is the reason only one steep drop in Sentry Function has been observed.

There are not a lot of research articles which can be compared with the provided results to justify the phenomenon. Davijani et. Al [4] has studied the Sentry Function on Glass Fiber Reinforced Plastic (GFRP) DCB Specimens and have observed discontinuous patterns in Sentry Function until failure. However, it should be understood that the Glass Fibers have significantly lower strength when compared to the Carbon Fibers and the energy required for Fiber Breakage or Fiber Pullout is low as well. Moreover, the specimen Davijiani et. Al used has a woven mid ply compared to the unidirectional plies in the presented study [4]. When the load is applied to the DCB specimen, the

Mode I delamination progresses along the direction of the fiber and thus we have one major damage at around 100 s and no major significant damages beyond that point. Summarizing the results, we can conclude that the material has lost its load carrying capability around 100 s duration.

3.4 WPT Results

The signal-based acoustic parameter, the waveform, carries information about the type of damage progression. Many researchers have reported the different frequency bands in the waveform that can be attributed to the different damage mechanisms [28, 39-40]. For instance, the Peak Frequency associated with Matrix Cracking is 125 kHz, Debonding is 200 kHz and Fiber Breakage can be associated with the Peak Frequency above 250 kHz.

It is quite impossible to present the Waveform Analysis for each Hit acquired during the Acoustic Events. For instance, in Specimen A, the total number of Acoustic Hits recorded during the DCB test is close to 20000. It means, necessarily there are almost 20000 waveforms recorded. Thus, based on the Load vs Time results, the region of damage progression in all the specimens was separated into three zones named Region 1, 2 and 3. From each Region, three hits were taken for WPT analysis. These Hits were not taken in random, nevertheless. The Hits taken for WPT analysis from each region represents the Peak Load in that specific region. However, in Specimen C there is no specific peak in Region 3. For this reason, 3 random hits at different time intervals from Region 3 were taken for analysis. The Cumulative Hits results were plotted over the DCB test results. For each specimen, a total of 9 Hits were taken for WPT analysis.

The WPT analysis was performed at the decomposition level i=3, thus obtaining a total of 2^i = 8 components. The decomposed WPT results for Specimen A, B and C are presented in Figures (11), (12) and (13), respectively.

The Energy content in each Wavelet Packet Level is an important parameter to be considered in the Frequency Analysis. To discriminate the different frequency band associated with the type of damage progression, the Energy content of each Frequency Band becomes an essential tool in damage characterization. The Energy Content and the Percentage of Each Energy Component has been calculated by Equations (2) and (3). Accordingly, for each region, there are 3 hits with a total of 9 hits for a Specimen. The Energy Content of each component in each specific hit for Specimen A, B and C has been provided in Table (1), (2) and (3), respectively.

Figure 11. *WPT Analysis of AE Hits in Specimen A*

WPT results in Figure 11, 12 and 13 shows the WPT decomposition results for the Wavelets accumulated during the testing of Specimen A, B and C, respectively. In Figure 11, the frequency band is predominantly between 150 kHz to 200 kHz region, thus, implying that the damage mechanism in Region 1 is predominantly due to Matrix Cracking and Debonding. In Region 2, again the frequency band is around 150 kHz however, the duration of the waveforms is rather longer. In Region 3, a different number of the short-ranged frequency band can be observed. This implies that in Region 3, the damage mechanism is an accumulation of Matrix Cracking, Debonding and Fiber Breakage. The Energy content of each frequency band can be decomposed and calculated using Equation (2) and (3) and is provided in Table 1. The exact percentage of the Energy Content in each Frequency Band can be evaluated and understood. It was underlined in the previous section that the slight unhinging of piano hinges was observed in the images recorded using CCD camera. While looking at the Region 2 in Figure 11, the waveform with uncharacteristic longer duration can be seen. This indicates that the acoustic activity at that point is different from the other instances. From which, we can confer that the longer duration signal represents the cracking in the adhesive holding the piano hinges. The frequency band in that region also around 150 kHz indicating that the damage propagation can be attributed only to matrix cracking.

Figure 12. *WPT Analysis of AE Hits in Specimen B*

Similarly, from Figure 12 and Table 2, the Energy Content of Specimen B can be seen. The majority of the Energy content lies above 400 kHz. Normally, only the Fiber Breakage occurs above the frequency of 250 kHz. It can be understood that some major damage propagation, possible, fiber breakage has occurred at a very early stage in Specimen B. This can also be confirmed by the lower Peak load and earlier stage of deterioration in Specimen B.

Figure 13. *WPT Analysis of AE Hits in Specimen C*

Table 1. *WPT Energy Content for Specimen A*

Table 2. *WPT Energy Content for Specimen B*

Table 3. *WPT Energy Content for Specimen C*

For Specimen C, from Figure 13 and Table 3, in Region 1 and 2, most of the Energy content lies within the two Frequency bands, 150 kHz and 200-250 kHz. However, in Region 3, about 27% to 35% of the Energy Content lies above 250 kHz. It can be observed in Region 3 the different short-ranged frequency bands. This confirms that the several damage mechanisms at Region 3 accumulated to the true failure of the material.

From the above observations, it can be inferred that the WPT is an online tool, which functions on Signal-based AE data and provides information on the Material characteristics not only at the critical point but also during the entire load history. It truly serves the purpose of the preventive monitoring of a Material. It provides very simple decomposition plots from which the initiation or propagation of damage can be easily identified. Apart from that, the false signals and critical stages of failure can also be monitored using WPT results. By categorizing the frequency band and time domain for each type of damage propagation, the false alarms can be easily identified.

4. Conclusion

Three double cantilever specimens (DCB) were tested and the mode I delamination characteristics were monitored by Acoustic Emission (AE) technique. The mechanical results show the variation in peak loads despite the specimens having the same geometrical and material characteristics. The variation in peak loads can be attributed to the curing mechanism and adhesive strength of the piano hinges attached to the specimens. The Sentry function was evaluated to compare the mechanical results with the acoustic activities. The damage progression and the critical point of failure can easily be identified by relating the Acoustic Energy with the Strain Energy using the Sentry function. Finally, the Wavelet Packet Transform (WPT) was used to decompose the signal-based AE parameter, the wavelets, to obtain information on the damage characteristics. Using the WPT analysis, it is possible to discriminate the frequency band associated with each damage mechanism and the percentage of energy content in each frequency band. Through this, the online monitoring of the damage progression in a material can be identified. With proper usage and development of the WPT analysis, it is possible to avoid the 'false signals' during an Acoustic activity.

5. References

1. Grosse C. Introduction. In: Grosse C., Ohtsu M. (eds) Acoustic Emission Testing. Springer, Berlin, Heidelberg, 2008.

2. Balázs GL, Grosse C, Koch R, Reinhardt HW. Damage accumulation on deformed steel bar to concrete interaction detected by acoustic emission technique. Mag of Concrete Research 1996;48:311-320.
3. Grosse C, Linzer L. Signal-Based AE Analysis. In: Grosse C., Ohtsu M. (eds) Acoustic Emission Testing. Springer, Berlin, Heidelberg, 2008.
4. Bakhtiary Davijani AA, Hajikhani M, Ahmadi M. Acoustic emission based on sentry function to monitor the initiation of delamination in composite materials. Mater Des 2011;32:3059–65.
5. Ativitavas N, Fowler T, Pothisiri T. Acoustic emission characteristics of pultruded fiber reinforced plastics under uniaxial tensile stress. In: Proceedings of European WG on AE, Berlin, 2004. p. 447–54.
6. Ciampa F, Meo M. A new algorithm for acoustic emission localization and flexural group velocity determination in anisotropic structures. Compos Part A-Appl S 2010;41:1777-1786.
7. Marec A, Thomasa JH, El Guerjouma R. Damage characterization of polymer-based composite materials: multivariable analysis and wavelet transform for clustering acoustic emission data. Mech Syst Signal Process 2008;22:1441–64.
8. Kharrat M, Placet V, Ramasso E, Boubakar ML. Influence of damage accumulation under fatigue loading on the AE-based health assessment of composite materials: Wave distortion and AE-features evolution as a function of damage level. Compos Part A-Appl S 2018;109:615-627.
9. Hamstad MA. Frequencies and amplitudes of AE signals in a plate as a function of source rise time. In: 29th European conference on acoustic emission testing. https://www.ndt.net/events/EWGAE%202010/proceedings/papers/20_Hamstad.pdf
10. Oz FE, Ersoy N, Lomov SV. Do high frequency acoustic emission events always represent fibre failure in CFRP laminates? Compos Part A-Appl S 2017;103:230-235.
11. Finkel P, Mitchell JR, Carlos MF. Experimental study of 'Auto Sensor Test-Self Test Mode' for acoustic emission system performance verification. AIP Conf Proc 2000;509:1995–2002.
12. Philippidis TP, Nikolaidis VN, Anastassopoulos AA. Damage characterization of carbon/carbon laminates using neural network techniques on AE signals. NDT&E Int 1998;31:329–340.
13. Benmedakhene S, Kenane M, Benzeggagh ML. Initiation and growth of delamination in glass/epoxy composites subjected to static and dynamic loading by acoustic emission monitoring. Compos Sci Tech 1999;59:201–208.

14. Godin N, Huguet S, Gaertner R. Integration of the Kohonen's self-organising map and k-means algorithm for the segmentation of the AE data collected during tensile tests on cross-ply composites. NDT&E Int 2005;38:299–309.
15. Barile C, Casavola C, Pappalettera G, Pappalettere C. Acoustic emission analysis of aluminum specimen subjected to laser annealing. In: Conference Proceedings of the Society for Experimental Mechanics Series, 8; 2014. p. 309-315.
16. Barile C, Casavola C, Pappalettera G, Pappalettere C. Analysis of crack propagation in stainless steel by comparing acoustic emissions and infrared thermography data. Eng Fail Anal 2015;69:35-42.
17. Minak G, Zucchelli A. Damage evaluation and residual strength prediction of CFRP laminates by means of acoustic emission techniques. In: Durand LP, editor. Composite materials research progress. New York: Nova Science Publishers Inc; 2008. p. 165–207.
18. Fotouhi M, Heidary H, Ahmadi M, Pashmforoush F. Characterization of composite materials damage under quasi-static three-point bending test using wavelet and fuzzy C-means clustering. J Compos Mater 2012;46(15):1795–808.
19. Pollard HF. Sound Waves in Solids, Pion Limited, London, 1977.
20. Ohtsu M. The history and development of acoustic emission in concrete engineering. Mag Concr Res 1996;48:321–30.
21. Pollock AA. Acoustic emission-2: acoustic emission amplitudes. Non-Destr Test 1973;6:264–269.
22. Hloupis G, Stavrakas I, Vallianatos F, Triantis D. A preliminary study for prefailure indicators in acoustic emissions using wavelets and natural time analysis, Proc Inst Mech Eng Part L: J Materials: Design and Applications 2016;230:780-788.
23. Vallianatos F, Michas G, Benson P, Sammonds P. Natural time analysis of critical phenomena: the case of acoustic emissions in triaxially deformed Etna basalt, Phys A 2013;392:5172-5178.
24. Hloupis G, Stavrakas I, Pasiou ED, Triantis D, Kourkoulis SK. Natural time analysis of acoustic emissions in Double Edge Notched Tension (DENT) marble specimens, Procedia Engineering 2015;109:248-256
25. Siron O, Chollon G, Tsuda H, Yamauchi H, Maeda K, Kosaka K. Microstructural and mechanical properties of filler-added coal-tar pitch-based C/C composites: The damage and fracture process in correlation with AE waveform parameters. Carbon 2011;39:2065–2075.

26. Ramirez-Jimenez CR, Papadakis N, Reynolds N, Gan TH, Purnell P, Pharaoh M. Identification of failure modes in glass/polypropylene composites by means of the primary frequency content of the acoustic emission event. Compos Sci Tech 2004;64:1819–1827.
27. Wickerhauser MV. Wavelet Packets. In: Adapted wavelet analysis from theory to software. A. K. Peters, Ltd. Natick, MA, USA, 1994.
28. Park JM, Kim HC. The effects of attenuation and dispersion on the waveform analysis of acoustic emission, J Phys D Appl Phys 1989;22:617-622.
29. Maillet E, Baker C, Morscher GN, Pujar VV, Lemanski JR. Feasibility and limitations of damage identification in composite materials using acoustic emission, Compos Part A Appl Sci Manuf 2015;75:77-83.
30. Ni Q, Iwamoto M. Wavelet transform of acoustic emission signals in failure of model composites. Eng Fract Mech 2002;69:717-728.
31. De Rosa IM, Santulli C, Sarasini F. Acoustic emission for monitoring the mechanical behaviour of natural fibre composites: A literature review. Compos Part A-Appl S 2009;40:1456-1469.
32. Understanding Wavelets. Part 4: An Example application of Continuous Wavelet Transform. From the series: Understanding Wavelets. www.mathworks.com
33. Barile C, Casavola C, Pappalettera G, Vimalathithan PK. Experimental Wavelet Analysis of Acoustic Emission Signal Propagation in CFRP. Eng Fract Mech 2019;210:400-407.
34. Mohammadi R, Saeedifar M, Toudeshky HH, Najafabadi MA, Fotouhi M. Prediction of delamination growth in carbon/epoxy composites using a novel acoustic emission-based approach. J Reinf Plast Comp 2015:34;868–878.
35. Barile C, Casavola C, Pappalettera G, Vimalathithan PK. Acousto-ultrasonic evaluation of interlaminar strength on CFRP laminates. Compos Struct 2019;208:796-805.
36. Yousefi J, Ahmadi M, Shahri MN, Oskouei AR, Moghadas FJ. Damage Categorization of Glass/Epoxy Composite Material Under Mode II Delamination Using Acoustic Emission Data: A Clustering Approach to Elucidate Wavelet Transformation Analysis. Arab J Sci Eng 2014:39;1325-1335.
37. Saeedifar M, Najafabadia MA, Zarouchas D, Toudeshky HH, Jalalvand H. Barely visible impact damage assessment in laminated composites using acoustic emission. Compos Part B-Eng 2018;152:180-192.

38. De Groot PJ, Wijnen AM, Janssen RB. Real-time frequency determination of acoustic emission for different fracture mechanisms in Carbon/Epoxy composites. Compos Sci Tech 1995;55:405-412.
39. Gutkin R, Green CJ, Vangrattanachai S, Pinho ST, Robinson P, Curtis PT. On acoustic emission for failure investigation in CFRP: pattern recognition and peak frequency analyses. Mech Sys Signal Pr 2011;25:1393-1407.
40. Barile C, Casavola C, Pappalettera G. Acoustic Emission Waveform Analysis in CFRP under Mode I Test, Eng Fract Mech 2019;210:414-421.

List of Figures and Tables

Figure Names:

Table Captions:

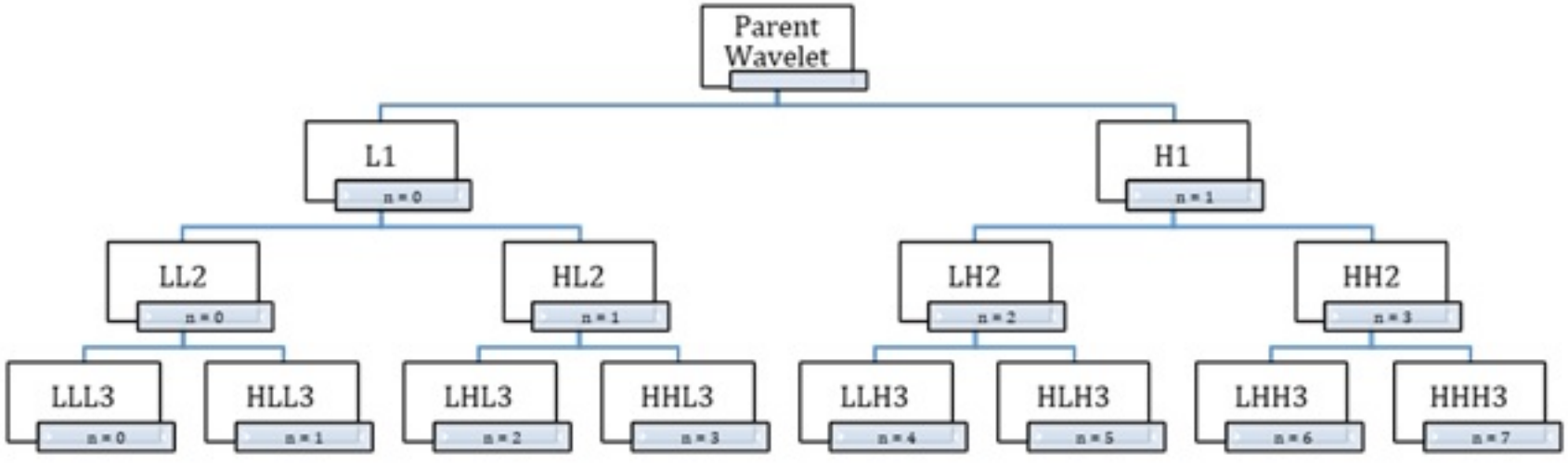
Parent Wavelet
L1
n = 0
H1
n = 1
LL2
n = 0
HL2
n = 1
LH2
n = 2
HH2
n = 3
LLL3
n = 0
HLL3
n = 1
LHL3
n = 2
HHL3
n = 3
LLH3
n = 4
HLH3
n = 5
LHH3
n = 6
HHH3
n = 7

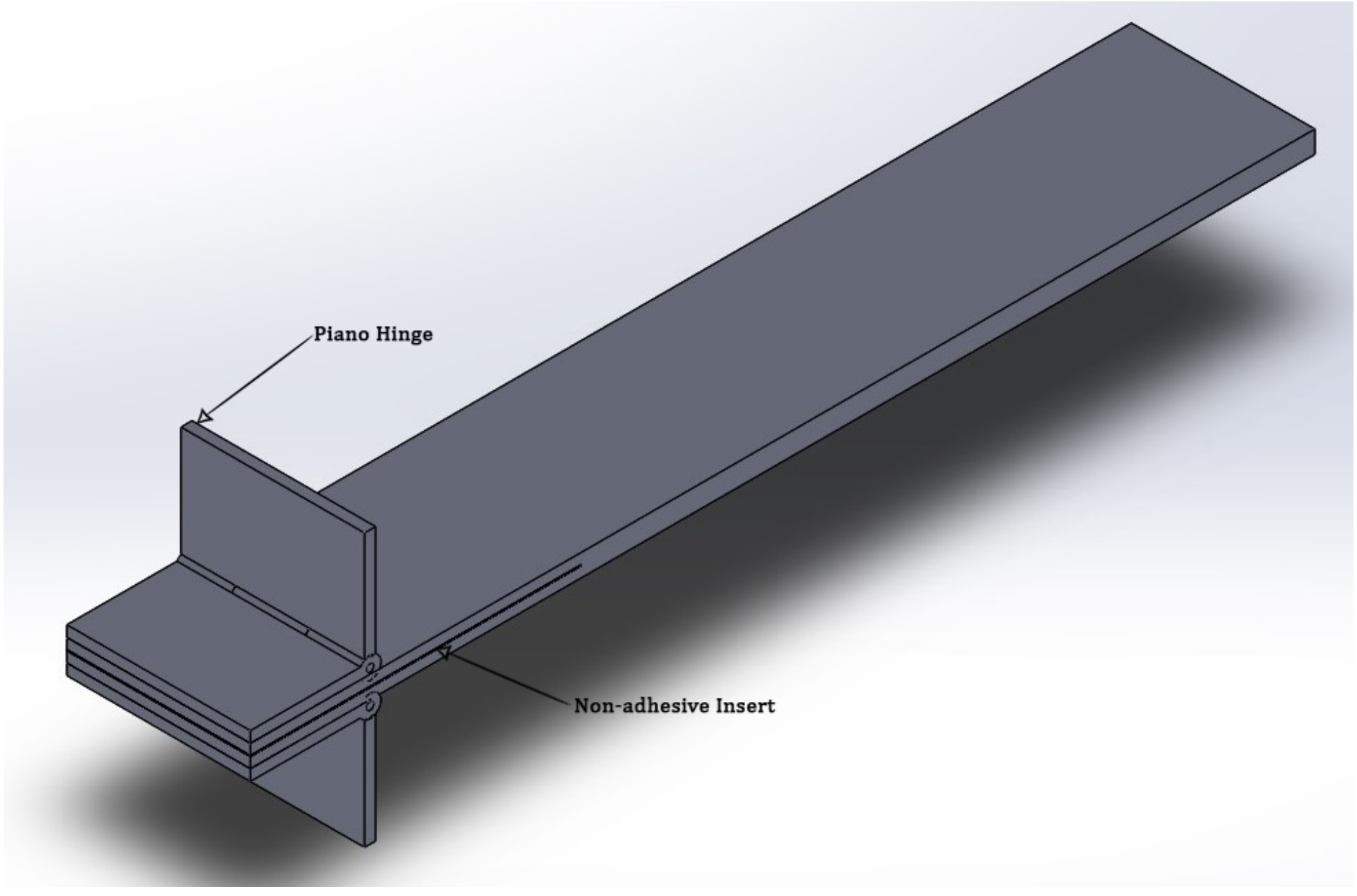
Piano Hinge
Non-adhesive Insert

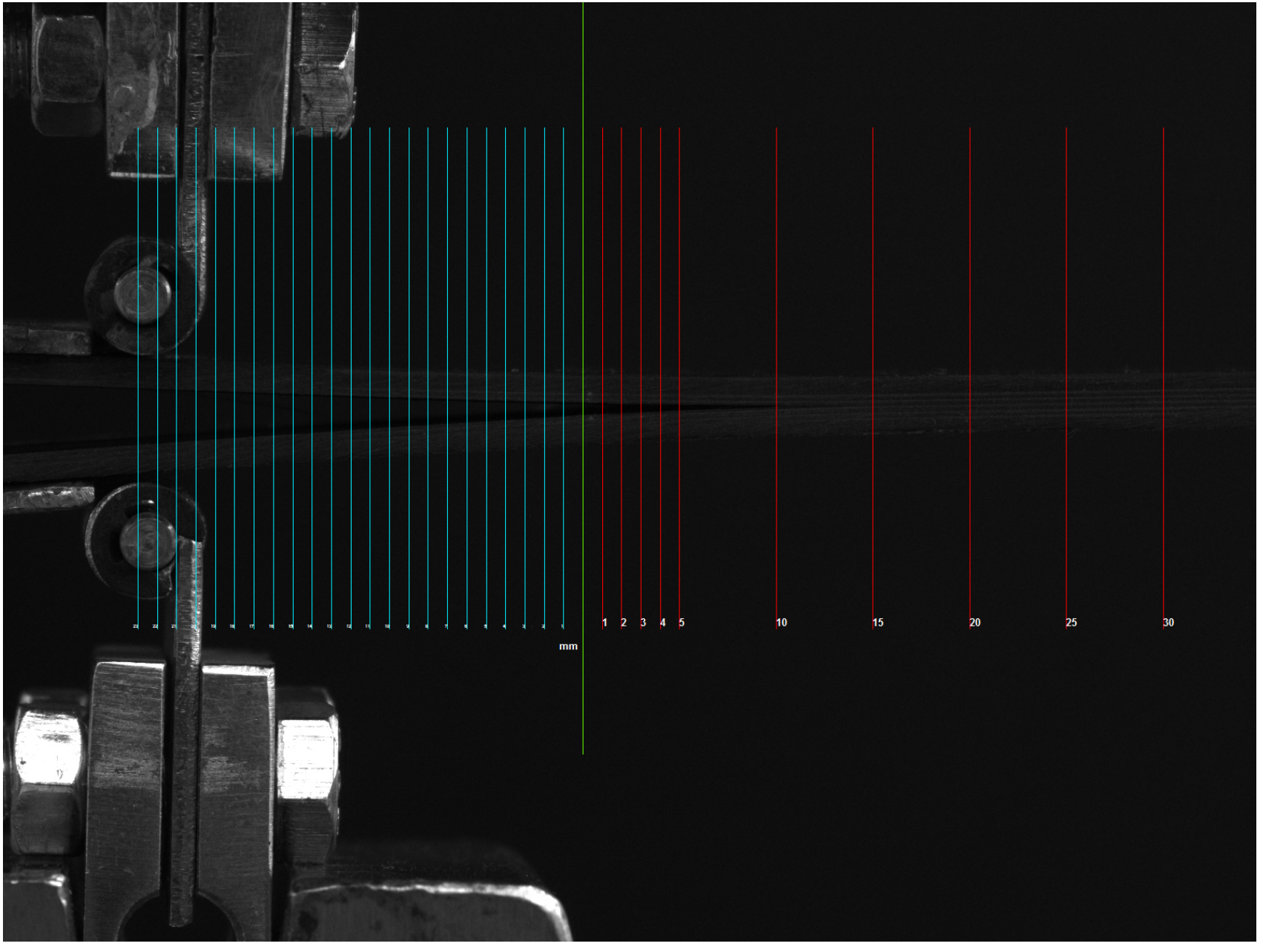
1
2
3
4
5
10
15
20
25
30
mm

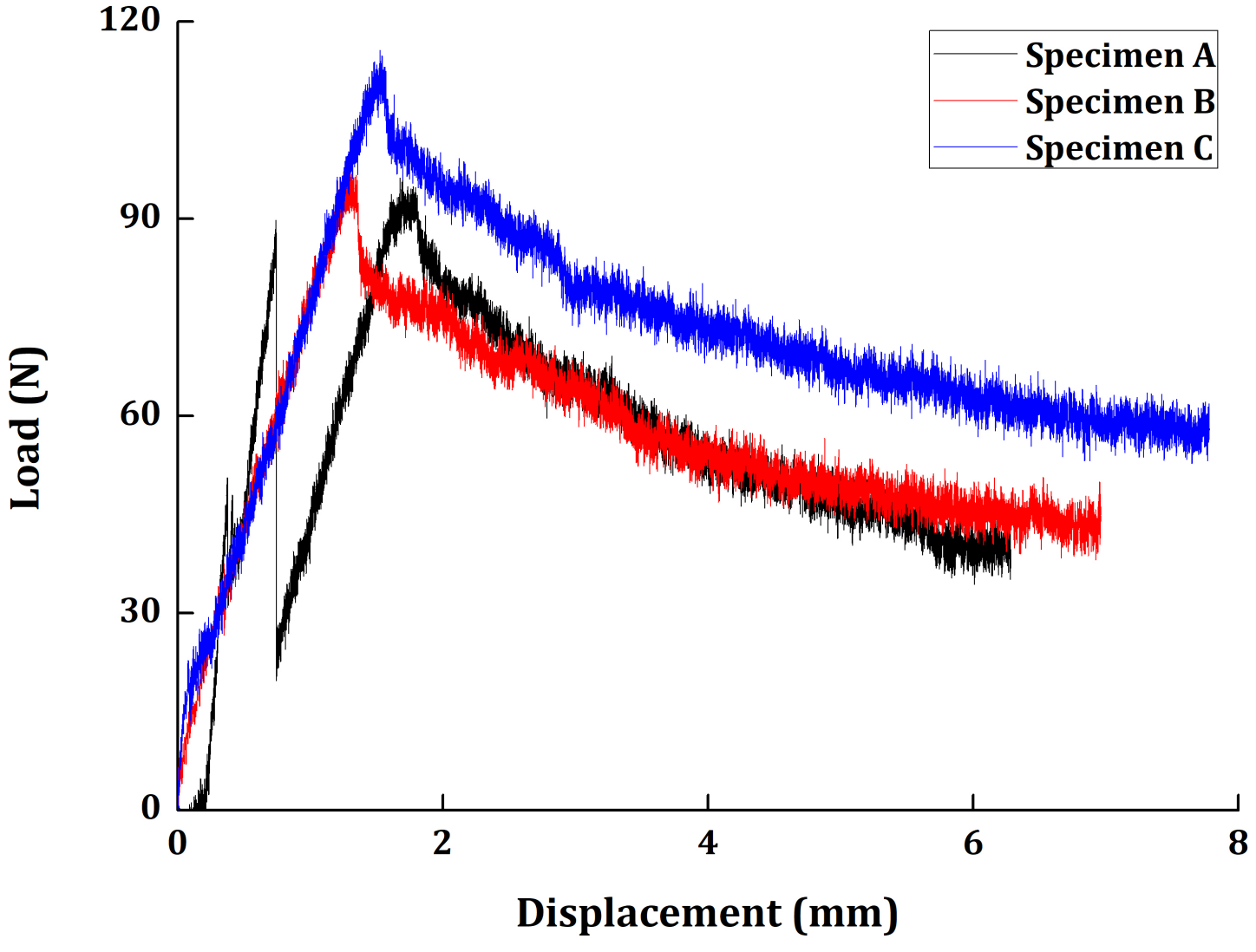
120
90
60
30
0
Load (N)
0
2
4
6
8
Displacement (mm)
Specimen A
Specimen B
Specimen C

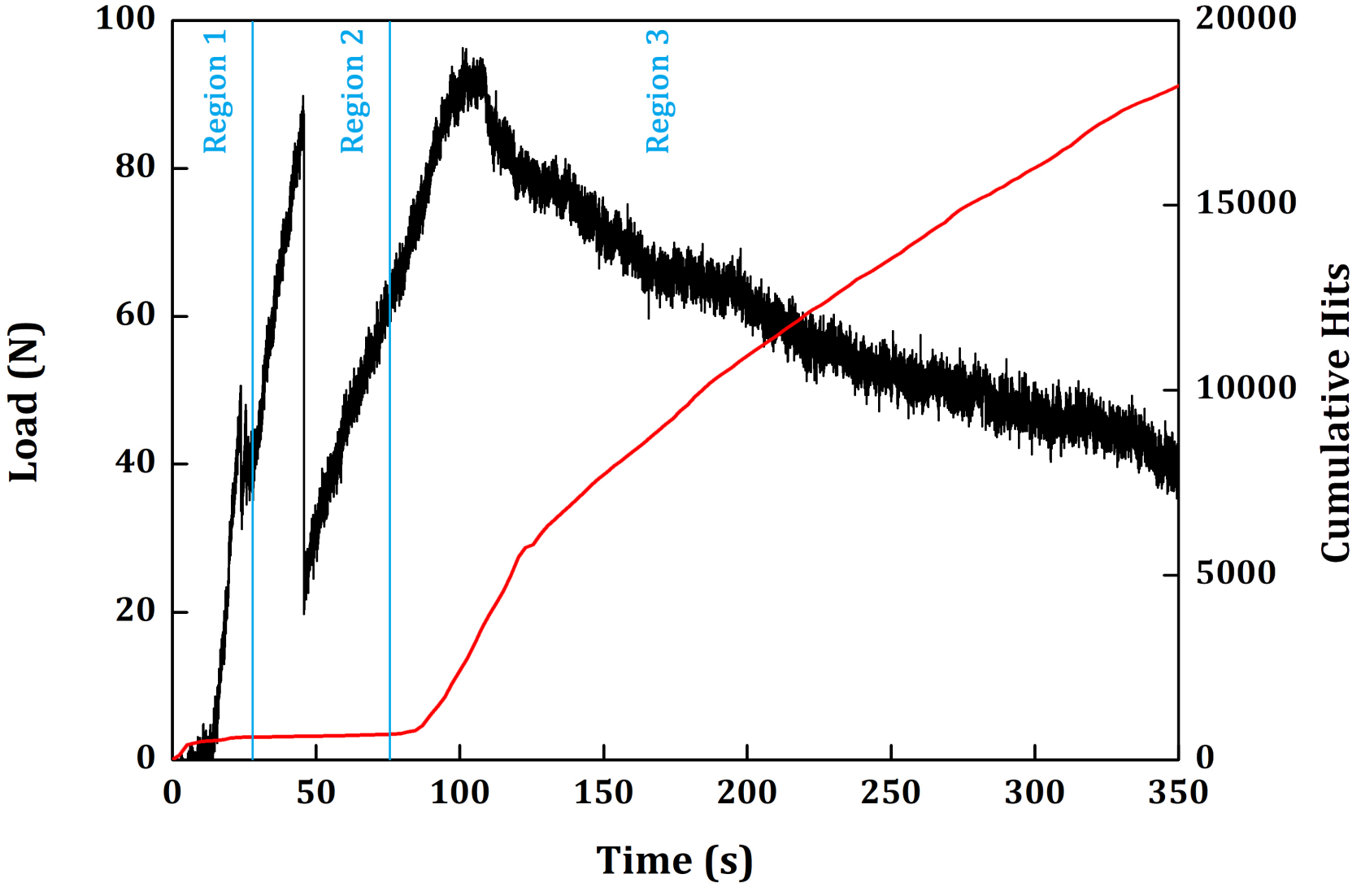
Region 1
Region 2
Region 3
Load (N)
Cumulative Hits
Time (s)
0
20
40
60
80
100
0
5000
10000
15000
20000
0
50
100
150
200
250
300
350

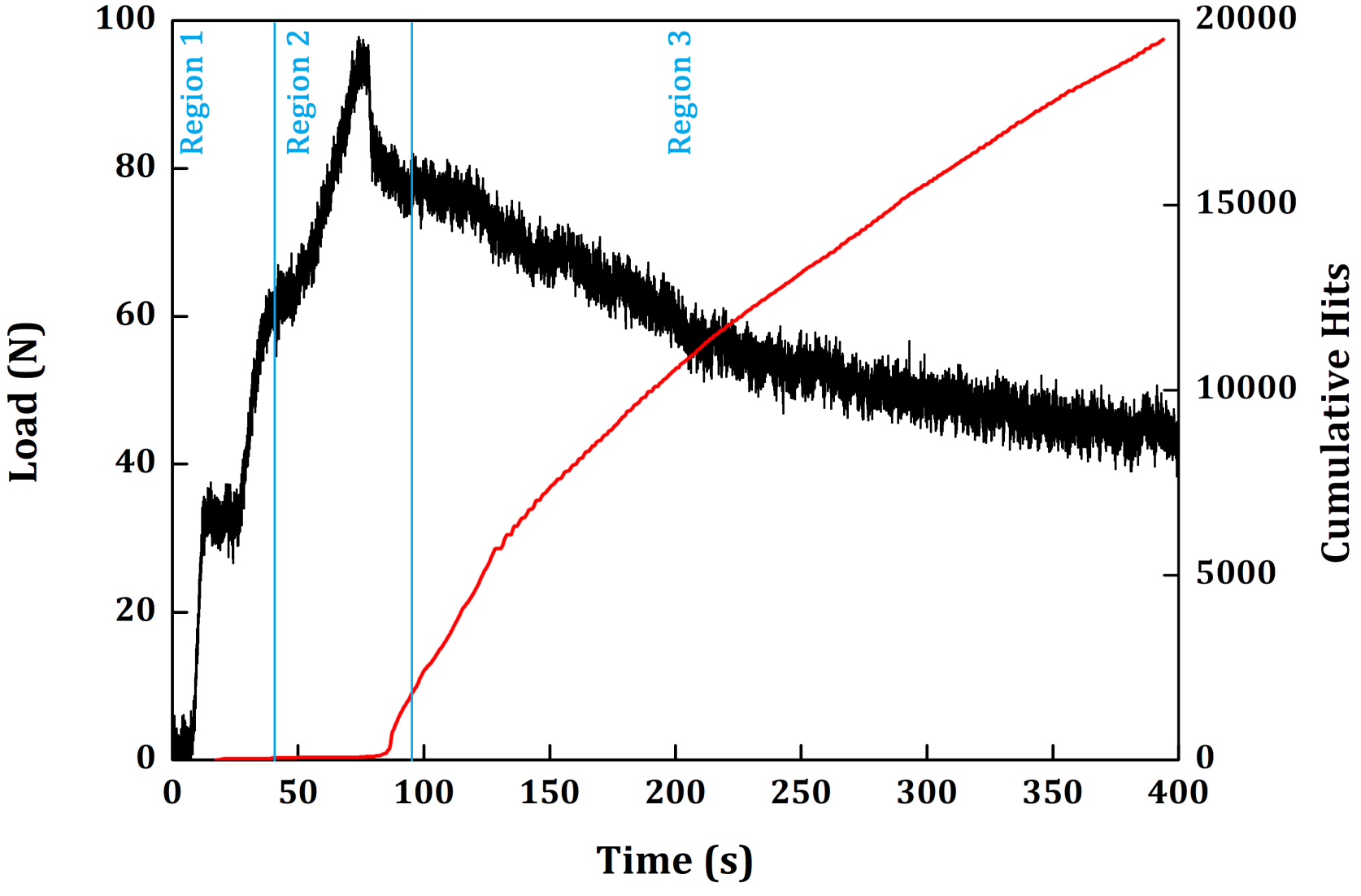
Region 1
Region 2
Region 3
Load (N)
Cumulative Hits
Time (s)
0
20
40
60
80
100
0
5000
10000
15000
20000
0
50
100
150
200
250
300
350
400

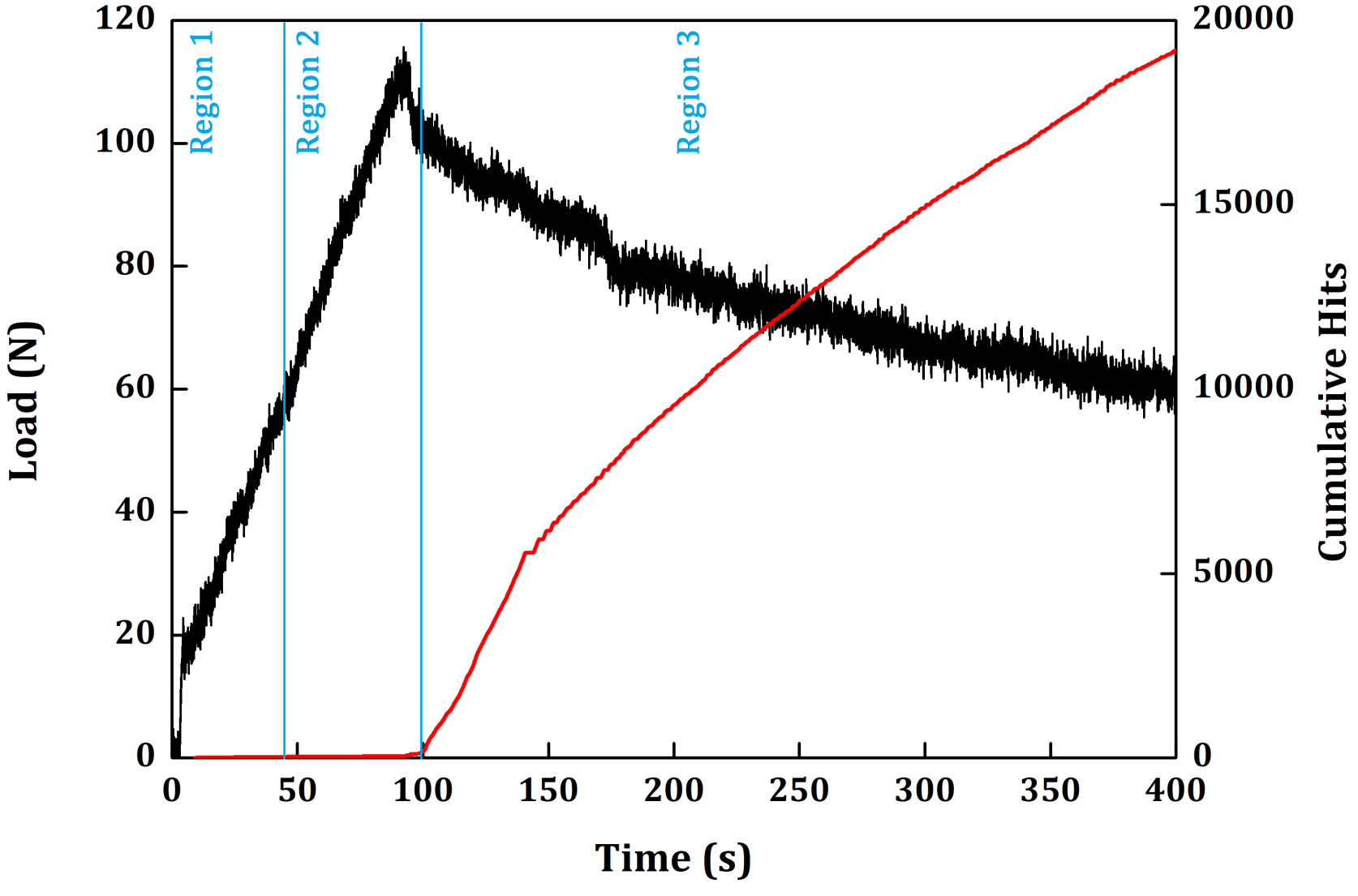
Region 1
Region 2
Region 3
Load (N)
Cumulative Hits
Time (s)
0
20
40
60
80
100
120
0
5000
10000
15000
20000
0
50
100
150
200
250
300
350
400

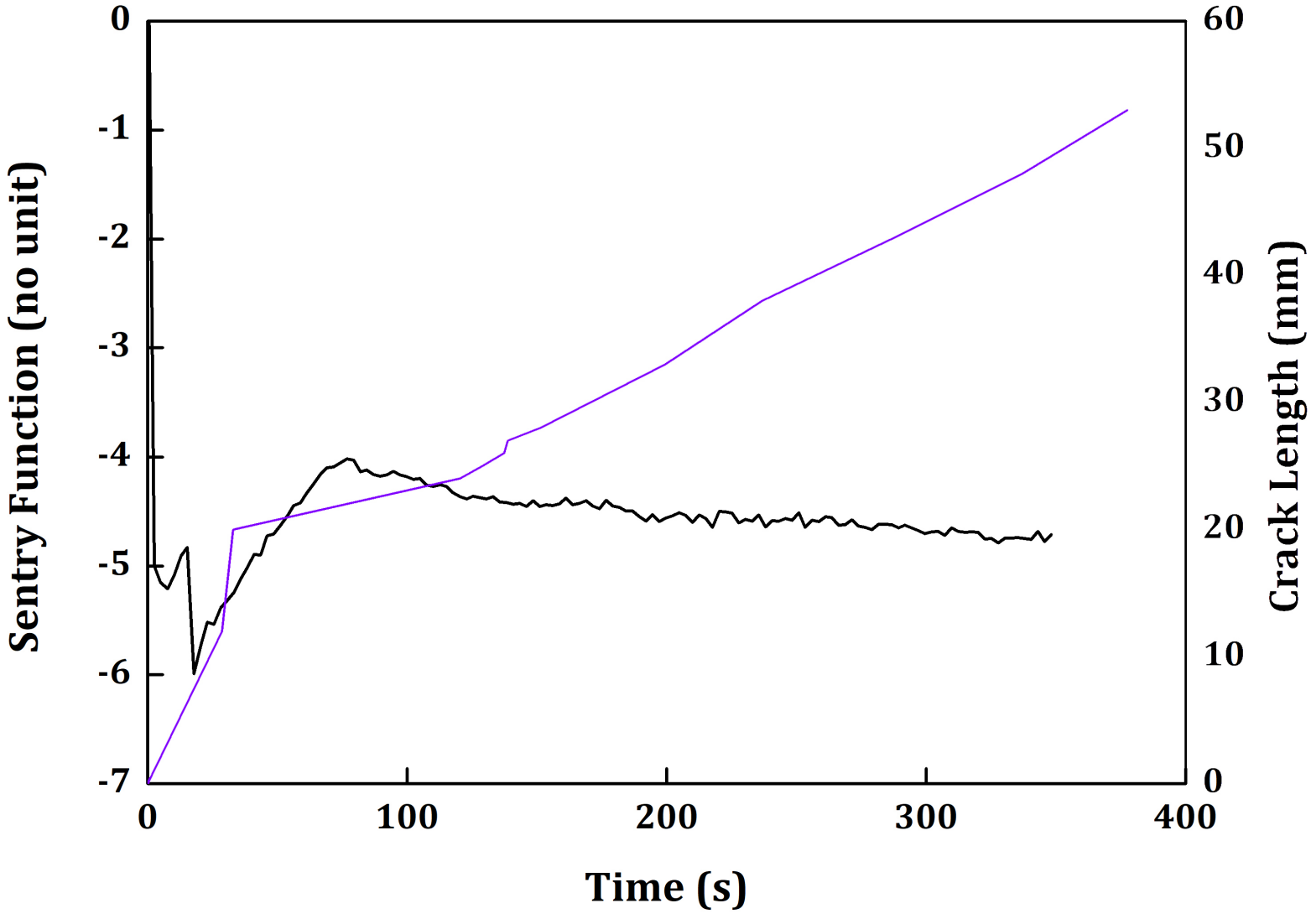
Sentry Function (no unit)
0
-1
-2
-3
-4
-5
-6
-7
Crack Length (mm)
60
50
40
30
20
10
0
0
100
200
300
400
Time (s)

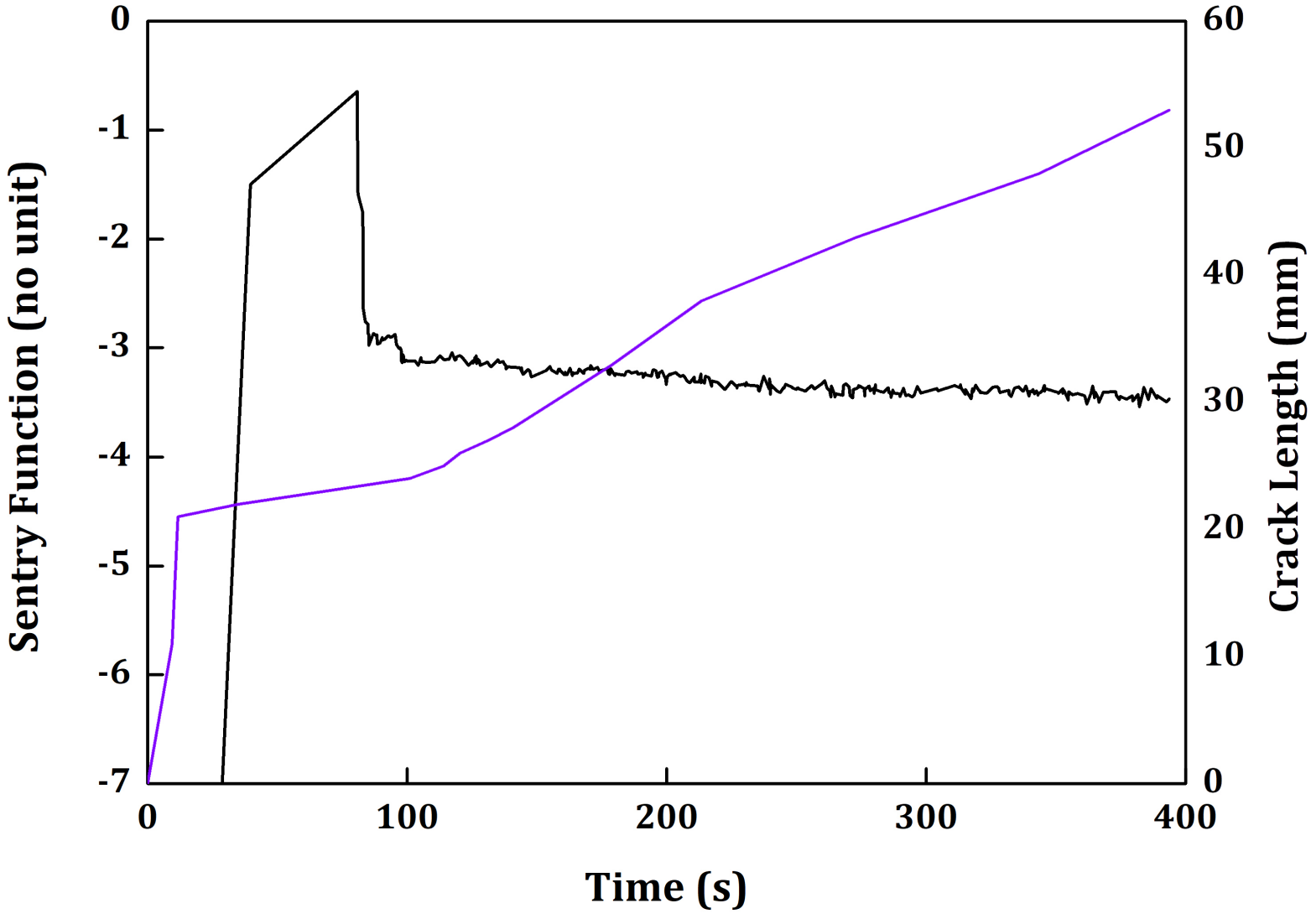
Sentry Function (no unit)
0
-1
-2
-3
-4
-5
-6
-7
Crack Length (mm)
60
50
40
30
20
10
0
0
100
200
300
400
Time (s)

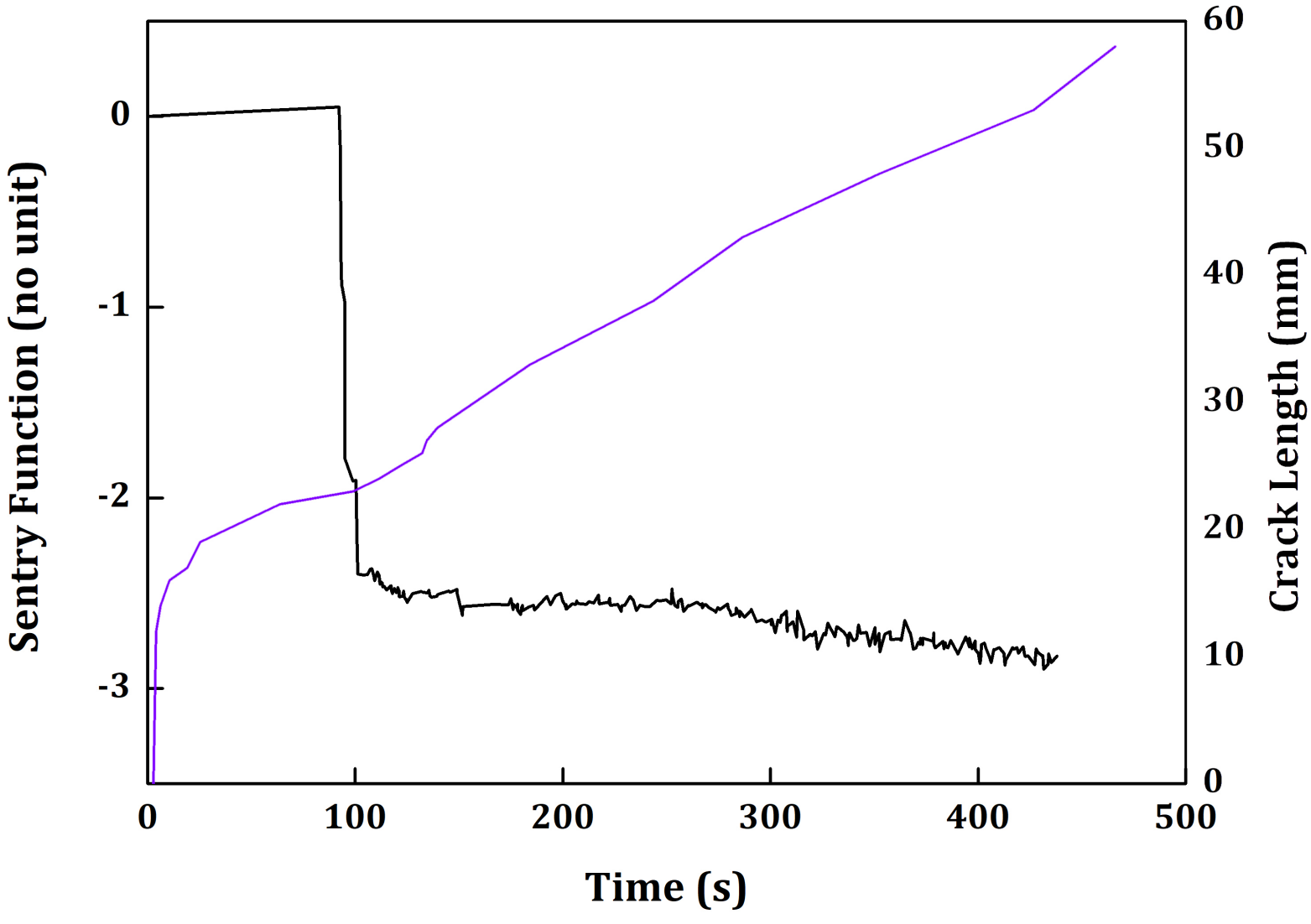
Sentry Function (no unit)
0
-1
-2
-3
Crack Length (mm)
60
50
40
30
20
10
0
0
100
200
300
400
500
Time (s)

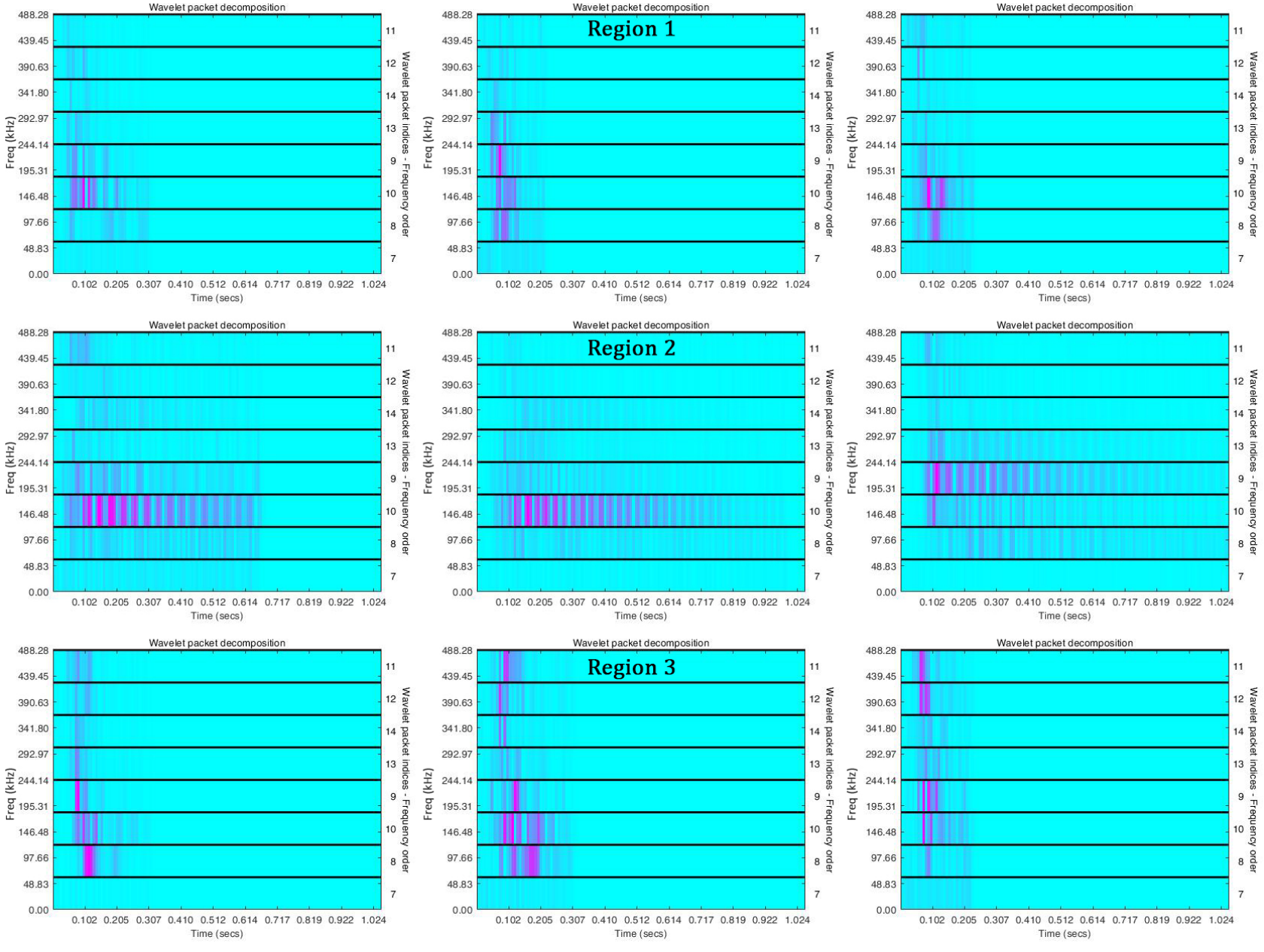
Wavelet packet decomposition
Region 1
Region 2
Region 3
Freq (kHz)
488.28
439.45
390.63
341.80
292.97
244.14
195.31
146.48
97.66
48.83
0.00
Wavelet packet indices - Frequency order
11
12
14
13
9
10
8
7
0.102 0.205 0.307 0.410 0.512 0.614 0.717 0.819 0.922 1.024
Time (secs)

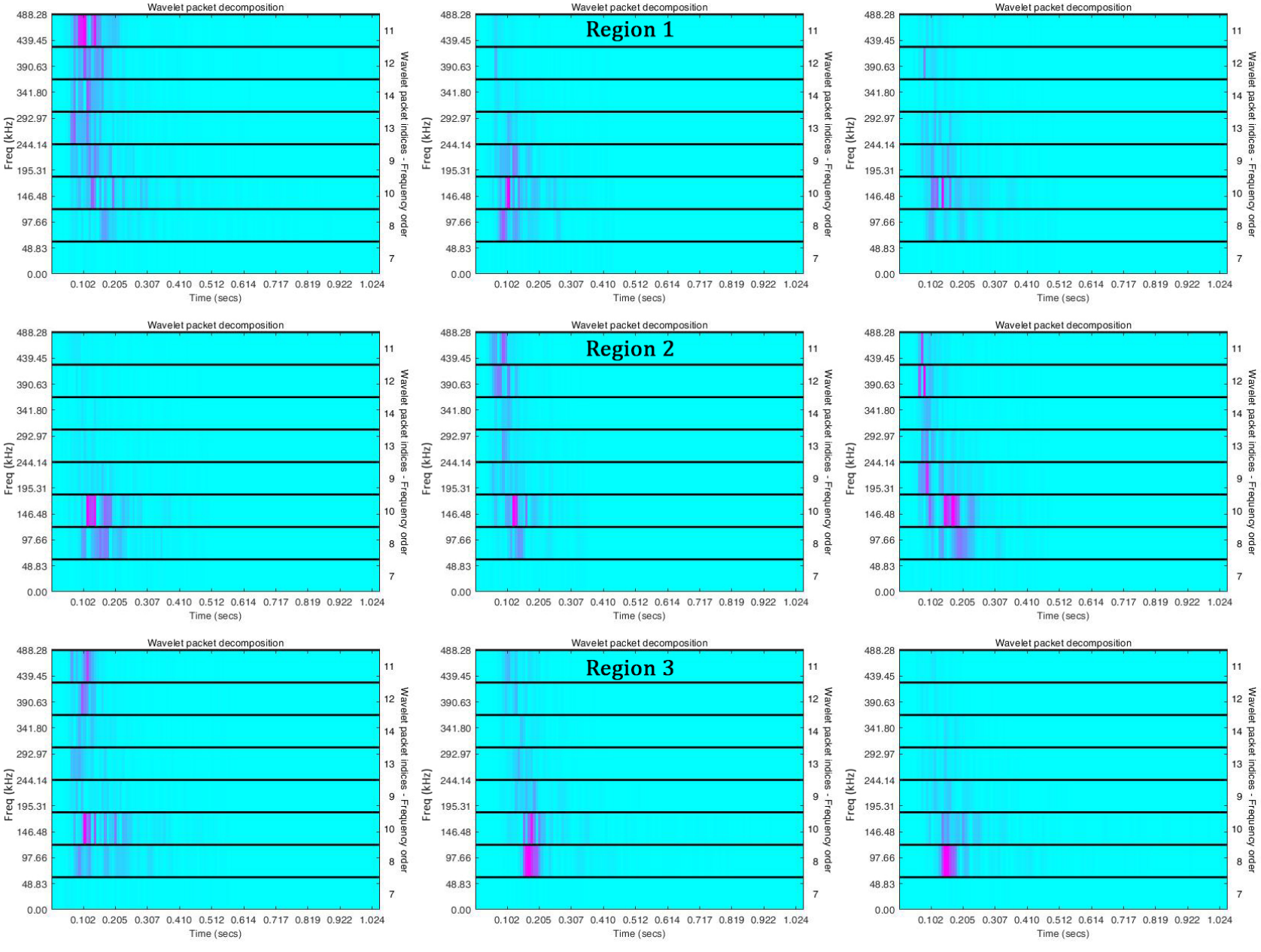
Region 1
Region 2
Region 3
Wavelet packet decomposition
Freq (kHz)
488.28
439.45
390.63
341.80
292.97
244.14
195.31
146.48
97.66
48.83
0.00
Wavelet packet indices - Frequency order
11
12
14
13
9
10
8
7
0.102 0.205 0.307 0.410 0.512 0.614 0.717 0.819 0.922 1.024
Time (secs)

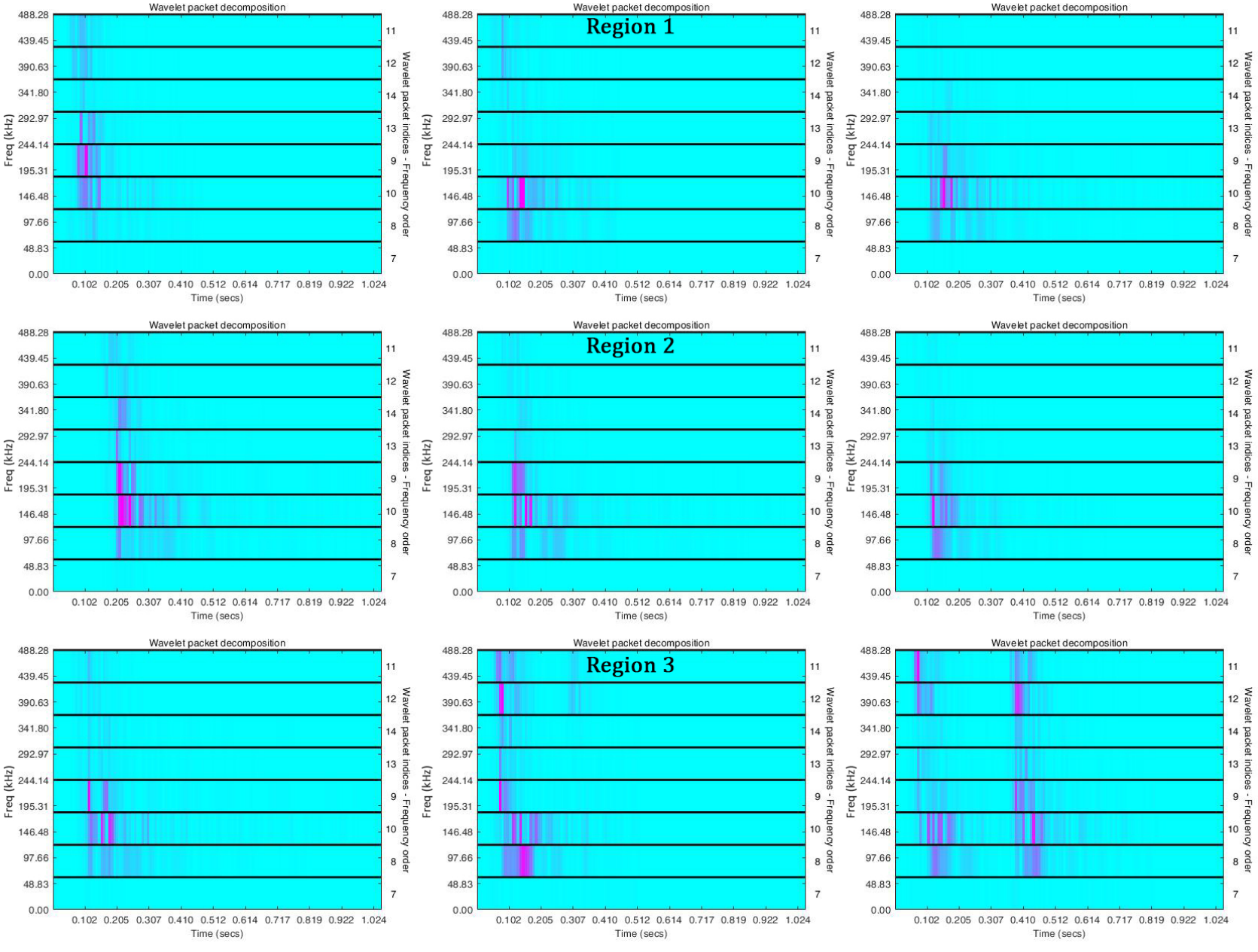
Wavelet packet decomposition
Region 1
Region 2
Region 3
Freq (kHz)
488.28
439.45
390.63
341.80
292.97
244.14
195.31
146.48
97.66
48.83
0.00
Wavelet packet indices - Frequency order
11
12
14
13
9
10
8
7
0.102 0.205 0.307 0.410 0.512 0.614 0.717 0.819 0.922 1.024
Time (secs)

Table 1. *WPT Energy Content for Specimen A*

Region	**Hit**	**Energy Content** (%)			
		Frequency (kHz)			
		0-100	**150**	**200-250**	**Above 250**
1	1	8.64	65.33	18.92	7.11
	2	27.11	27.18	40.13	5.58
	3	26.52	54.31	9.98	9.18
2	4	7.73	74.58	11.44	6.26
	5	5.69	82.61	8.33	3.37
	6	11.1	15.4	69.33	4.17
3	7	36.06	24.6	26.17	13.17
	8	27.36	32.78	16.47	23.39
	9	6.68	22.23	34.44	36.65

Table 2. *WPT Energy Content for Specimen B*

Region	Hit	Energy Content (%)			
		Frequency (kHz)			
		0-100	150	200-250	Above 250
1	1	4.26	12.19	20.10	63.45
	2	27.23	44.33	24.43	4.01
	3	10.01	61.64	18.65	9.70
2	4	28.47	67.03	3.09	1.41
	5	9.97	42.85	10.36	36.82
	6	15.23	42.88	19.39	22.51
3	7	12.55	42.78	8.45	36.21
	8	54.52	29.80	8.56	7.12
	9	72.38	19.57	6.37	1.68

Table 3. *WPT Energy Content for Specimen C*

Region	Hit	Energy Content (%)			
		Frequency (kHz)			
		0-100	100-150	200-250	Above 250
1	1	2.61	26.92	59.14	11.33
	2	22.61	65.93	4.53	6.93
	3	11.69	73.60	13.67	1.04
2	4	6.84	55.77	28.19	9.20
	5	14.92	51.24	31.65	2.19
	6	29.05	56.29	13.83	0.83
3	7	13.13	52.86	29.87	4.14
	8	33.37	24.93	14.91	26.79
	9	16.24	33.08	15.74	34.94